GEOPHYSICS, VOL. 70, NO. 2 (MARCH-APRIL 2005); P. T29–T44, 16 FIGS., 2 TABLES.
10.1190/1.1897039

Energy balance of a drill-bit seismic source, part 2: Drill-bit versus conventional seismic sources

Flavio Poletto[1]

ABSTRACT

The radiation properties of a downhole drill-bit seismic source are related to the amplitude and frequency of the forces exerted by the working bit. The main vibration modes of roller-cone and polycrystalline diamond compact (PDC) bits are investigated under different drilling conditions. The analysis includes vibrations produced by teeth indention, multilobed patterns, bouncing with periodic and random effects, single-cutter forces, stick-slip and whirling effects, mud-pressure modulation forces, and bit wear. Drill-bit radiation properties are calculated using the results obtained in part 1 of this paper and are numerically compared to the radiation of conventional vertical seismic profiling (VSP) sources.

INTRODUCTION

This paper is the second part of a work on drill-bit seismic while drilling (SWD) energy balance. Part 1 (Poletto, 2005, this issue) focuses on rotary energy and drill-bit radiation properties. It analyzes energy requirements of the drilling process, radiation properties of the drill-bit source, and near-field effects to scale the energy expended by the bit in lateral gouging and vertical rock penetration. In particular, part 1 analyzes radiation of waves in the far-field, near-field effects, and downhole vibrations caused by a single vertical (or axial) force. In real drilling conditions, drill-string downhole vibrations at the bit are caused by many factors, including transverse forces, beats from irregular rotation at the bit, normal and anomalous vibration modes of the drill string, and modulation caused by fluctuation of mud pressure with frequency of the pump strokes.

Part 2 analyzes the drilling conditions and vibration modes that affect drilling and contribute to increasing the level of downhole string vibrations. In particular, part 2 analyzes the main periodic and nonperiodic random forces of rotary bits acting as a source of vibrations radiated in the formation and induced in the drill string.

The drill bit, under the weight loaded by the drill string, transforms most of the rotary energy into the action of breaking rock and a small percentage of the energy into radiated-vibrations energy (part 1). Different types of drill bits — of different shapes and mechanical action — can be used to drill a well. The most common are roller-cone bits (also called tricone or rock bits) and bits with fixed cutter inserts — namely, diamond and polycrystalline diamond compact (PDC) bits. Special core bits are designed to retrieve plug-shaped sample cores of rock. The criterion of bit-type selection from hundreds of different drill bits for a given drilling plan is related to factors such as expected drilling-rate performance, cost per unit depth, and bit life. The action of the different bit types characterizes the vibrations produced while drilling and the signal used for SWD purposes. This paper describes the layout of the main drill-bit types and their working action, including conditions of bouncing, whirl, and stick-slip.

ROLLER-CONE BITS

The roller-cone bit has cones with teeth that are designed to break rock by indention and gouging action. As the cones roll across the bottom — at least ideally, as true roll is never achieved — the teeth press against the formation with enough pressure to exceed the failure strength of the rock which fractures the rock (Devereux, 1999).

Examples of roller-cone bits are shown in Figure 1. The lower part of the body supports the roller cones — usually three (but also one, two, or four can be used). Each cone has two or three rows of teeth that (a) can be milled from the same block of metal as the bit (noninsert bit) and are used in relatively soft formations found at shallow depths (Langenkamp, 1994) or (b) can be of tungsten inserts, which are harder and more durable than milled teeth. The external, intermediate, and internal rows of a cone each have a different number of teeth. Each tooth is like a chisel and has a maximum height

Manuscript received by the Editor December 17, 2001; revised manuscript received April 21, 2004; published online March 22, 2005.
[1]Istituto Nazionale di Oceanografia e di Geofisica Sperimentale (OGS), Borgo Grotta Gigante 42/c, 34010 Sgonico Trieste, Italy. E-mail: fpoletto@ogs.trieste.it.

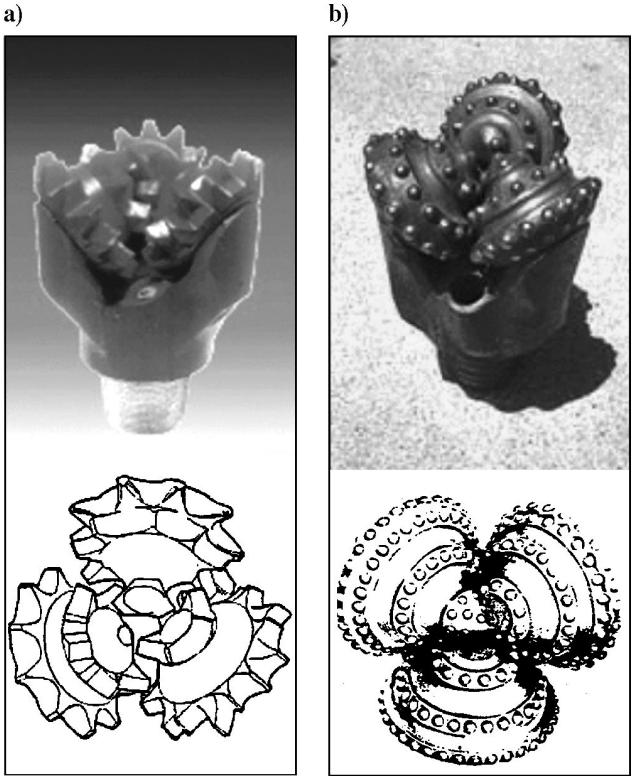

Figure 1. (a) Milled roller-cone bit used in softer and shallower formations. (b) Insert roller-cone bit used in deeper and harder formations.

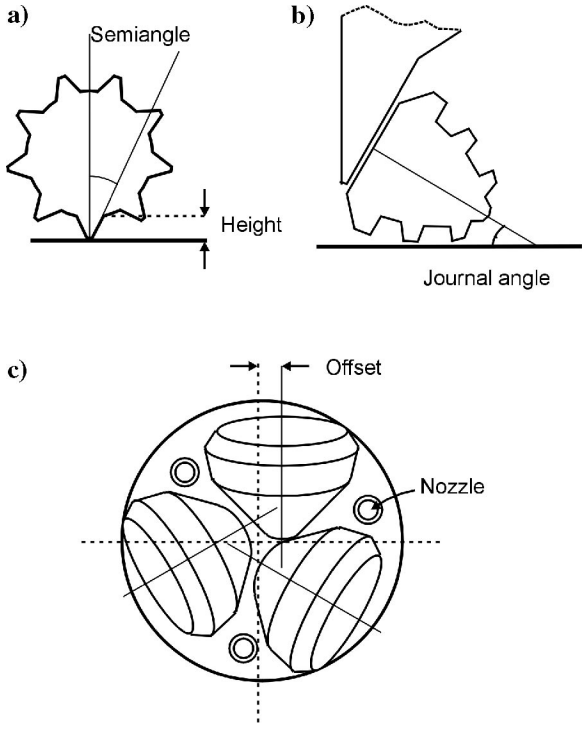

Figure 2. (a) Layout of a cone row. The tooth has a height h. (b) Journal angle formed by the bearing cone axis and the horizontal (or orthogonal to drilling axis) plane. (c) Offset of the cones and mud ejection nozzles. Modified after McGehee et al. (1992a).

(penetration depth) and a semiangle (the angle made by its lateral surface with the bit axis; Figure 2a). The wedge of a new tooth can be sharp or flat. Each cone is protected externally by the lobed body of the bit legs. The cones are supported by bearings, which are lubricated and sealed. The bearing axis of the cone forms the cone journal angle with the horizontal level (or normal to the bit axis; Figure 2b). The offset is the distance between the cone axis and the axis passing in the bit center. When the three cone axes meet in the bit center, the offset of the bit is zero (Figure 2c).

Eronini et al. (1982) assume a predominant shear model for the rock fracturing process (see equation 53 of part 1), where the roller bit is a nonideal transformer which destroys the rock through a teeth indention/fragmentation sequence. The energy for the indention (minor fracturing) comes from the incident weight on the bit, while the fragmentation energy (major fracturing) is derived from rotary gouging power. The teeth of the indentors of the inner rows of a roller-cone bit perform a gouging-scraping action, which is opposite that of the outer row. Sheppard and Lesage (1988) measure the transverse horizontal gouging backward force that the indentors of the inner row produce, which is, on average, opposite to the transverse force of the outer row. They also measure the resulting transverse couple between the inner and outer rows of a single cone. Nonzero offsets increase the gouging and scraping action as well as the deviation from the true roll of the bit (Ma and Azar, 1985), resulting in a sliding motion proportional to the cone offset (Winters et al., 1987). Indention and gouging energies are calculated in rotary drilling equation 52 of part 1 to estimate the fraction of percussive-indention energy.

The bit is provided with tungsten carbide nozzles (Figure 2c), which are located between the cones and through which the mud flowing into the pipes is ejected at high pressure. The mud has many functions: It cleans the bit and the hole of drilled-rock cuttings, removes heat, helps the cone rotate, and improves drilling hydraulic performance. The mud ejection directed against the rock can be regulated by using different nozzle sizes and geometries, thus making it possible to change the cleaning force and the pressure distribution under the bit and improve drilling performance (White and Curry, 1988).

In exploratory oil wells, roller bits may be preferred over diamond or PDC bits, which drill by cutting and grinding the rock into thin dust. In this case, the residual solids transported to the surface by the mud flow cannot be interpreted by well-site geologists as effectively as cutting chips.

ROLLER-CONE BIT AS A PERIODIC VIBRATION SOURCE

Using the radiation analysis developed in part 1, I assume that the radiation impedance to the bit-axial single force is not influenced by lateral and torsional vibrations. I show below that the roller-bit source produces sufficient vibration energy for SWD purposes, which is comparable to that of conventional seismic sources. This agrees with application results (Rector and Marion, 1991; Miranda et al., 1996), which show that, in general, roller-cone bits produce compressional seismic components of sufficient energy for check-shot analysis, prediction ahead of the bit, and while-drilling imaging by depth migration of multioffset data. When drilling hard

formations with a tricone bit, two kinds of drill-string axial vibrations appear (Yang, 1990). One is the high-frequency vibration caused by the teeth of the cones; the other is the low-frequency vibration caused by the lobed-bottom shape of the hole. A related axial vibration not from the bit action is pulsation attributable to mud-pump pressure fluctuations (Cunningham, 1968).

Vibrations induced by teeth indention

Ma and Azar (1985) have studied the dynamics of roller-cone bits to determine the number of teeth in contact with the bottom of the hole and their instantaneous position and velocity. The tests they use indicate that penetration depth versus bit revolution is not a smooth, straight line but is a broken line with transition steps, shaped like a staircase (Figure 3). However, in this analysis it is unclear which boundary conditions in the drilling system may influence the bit vibrations and performance. The tests show that, after revolving a certain number of turns, when all the craters over the bottom are formed, the roller bit suddenly drops down. The drop distance equals the average crater depth and can be calculated easily as the average rate of penetration (ROP) per turn multiplied by the number of turns necessary to drop down a step. After dropping, the bit revolves at the new depth level until the next drop. During this process, the top of a tooth will not leave the bottom of the excavated crater until the next tooth (not necessarily of the same row) is the new instantaneous rotation center (Figure 4). Ma and Azar (1985) conclude that the instantaneous positions and velocities at each moment of the teeth being in contact with bottom are, in practical application, unknown.

Sheppard and Lesage (1988) calculate the (nonlinear) equations governing the force-penetration relations for a single cone by assuming zero-torque moment around the journal-bearing axis and by balancing the total weight on bit (WOB) loaded on all the indentors in contact with the formation. For a full tricone bit, two additional equations are required to balance the total force on the three cones and the torque couple moment of each axis. In real drilling conditions, it is difficult to calculate the complete equations to determine the time evolution of the forces at the teeth of the bit. Because one tooth is disengaged from rock contact only when another tooth is engaged, the bit itself could be considered a multipole seismic source. But because the multipole random effects are distributed around the bit rotation angle, they can be neglected, and a simple vertical force can be used as a source model for our purposes — as discussed in part 1.

In a simplified interpretation model of the tricone bit, Sheppard and Lesage (1988) assume that only one rolling indentor per cone contacts the rock row at a given instant and that the total load is equally distributed on the three cones. These researchers study in detail the periodic force at the teeth of a drilling roller-cone bit. They use a fully instrumented bit cone to measure in the laboratory the forces on the inner and outer rows separately, as well as to determine the torque and the single indentor position during cone rotation. Sheppard and Lesage (1988) model and measure the vertical and horizontal forces versus vertical penetration and horizontal displacements. The vertical penetration of a single indentor tooth can be related to the vertical force by equation 51 (part 1):

$$F(x_p) = \sigma_p \tan \Theta x_p, \tag{1}$$

where F is the vertical force per unit chisel length, σ_p is the penetration strength, Θ is the tooth semiangle, and x_p is the distance penetrated by the bit tooth. (A quadratic relation can be calculated for the transverse horizontal action.) Sheppard and Lesage (1988) analyze the rolling and scraping action of the single cone and single indentors when drilling rock specimens. They represent the results versus the rotation angle of the cone about the journal bearing axis (giving cycles per cone revolution). They show that the mean rotation rate of the cone is 1.25 to 1.31 times the rotation rate of the bit around its vertical axis. In addition, they observe that, during the extraction phase, the indentor experiences an elastic restitution with slope $\arctan(\alpha_x x_p)$, where $\alpha_x \sim 5$, as determined in single indentor experiments (Figure 7, part 1).

The results of Sheppard and Lesage (1988) are used by Hardage (1992) to describe the periodic action of the roller-cone source. Figure 5a shows the vertical force of the 19-tooth outer row versus the cone rotation angle. Figure 5b shows the periodic force of the 9-tooth inner row in a complete turn (360°). These axial forces can be approximated by a periodic force of the type

$$F(t) \approx F_m + F_0 \sin \omega_{\text{row}} t, \qquad (F_m \geq F_0), \tag{2}$$

where t is time and where the mean F_m and the dynamic F_0 forces are given by

$$F_m = \frac{F_{\max} + F_{\min}}{2} \tag{3}$$

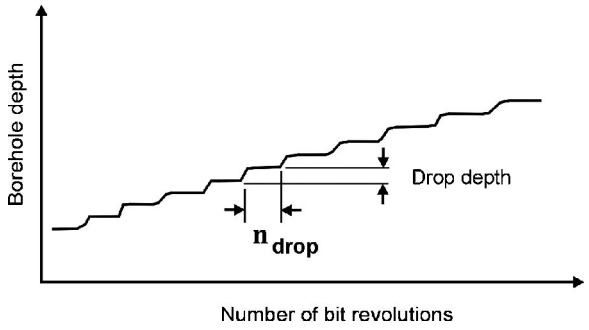

Figure 3. Roller-bit penetration versus number of bit revolutions. The drop distance is drilled in n_{drop} revolutions. Modified after Ma and Azar (1985).

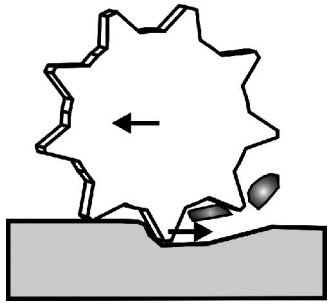

Figure 4. Tooth indention and gouging cutters. The tooth indenting the rock becomes the instantaneous center of rotation of the cone.

and

$$F_0 = \frac{F_{\max} - F_{\min}}{2}. \quad (4)$$

The terms $F_{\max}$ and $F_{\min}$ are the maximum and minimum load forces on the row, respectively (Figure 6a), and ω_{row} is the angular frequency of the force of the given row of teeth. Equation 2 is an approximation which does not include harmonic effects that account for the mode-coupling and bit-wear effects considered in this paper. Figures 5c and 5d show the forces during single indention events. A faster variation in the force during unloading (Biggs et al., 1969) can be observed after the maximum peak of the signal of the inner row, with a slope about five times that observed during loading. As discussed in part 1, the faster instantaneous variation of force (dF/dt) causes an increment in the average radiated energy. The synthetic example of Figure 6b is obtained with a modified sine function in which the unloading frequency is five times faster than the loading frequency. As calculated by equations 29 and 22 of part 1, the average radiated energy obtained by using this force is three times the average energy of the monofrequency harmonic force.

Sheppard and Lesage (1988) also show full-scale drilling results obtained by using $8\frac{1}{2}$-in. milled-tooth bits plotted versus dimensionless drilling parameters (see part 1). Since the original drilling parameters are unknown, the rotary drilling equations 1 and 52 of part 1 cannot be used to calculate energy from these literature data. Nevertheless, the results can be used to estimate the magnitude and frequency of the vertical (axial) force and to calculate the energy radiated into the far-field by the source, assumed to be a vertical force (equation 22, part 1) with the hypothesis that the peak-to-peak dynamic force component $2F_0$ is comparable to the maximum force magnitude $F_{\max}$.

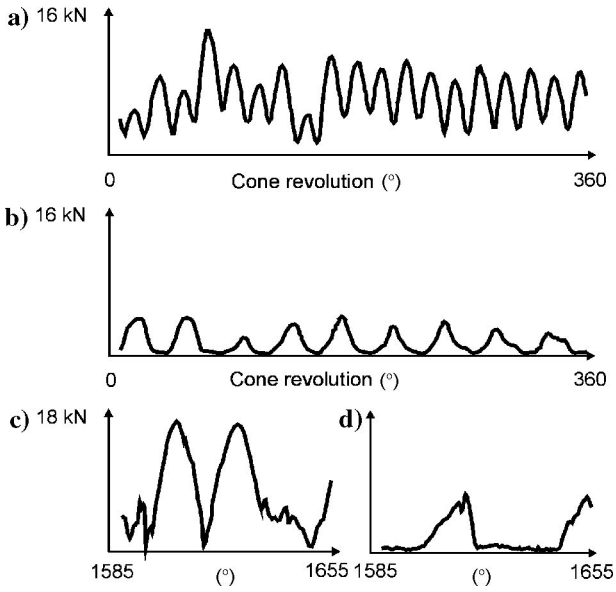

Figure 5. (a) Outer 19-tooth-row force versus cone revolution angle. (b) Inner 9-tooth-row force versus cone revolution angle. (c) Outer-row single events. (d) Inner-row single events. Modified after Sheppard and Lesage (1988).

Vibrations induced by lobed patterns

Field measurements show that cone bits frequently bounce off the bottom in both rotary drilling and turbo drilling (Cunningham, 1968; Wolf et al., 1985; Yang, 1990). Drill-string fluctuations have been observed at three times the rotary speed in revolutions per minute (3 × rpm) while drilling with tricone bits or, more generally, at the frequencies

$$f_{\text{LP}} = n\frac{\text{rpm}}{60}, \quad (5)$$

where the subscript LP is lobe pattern and n is an integer multiple of the number of cones (Skaugen, 1987). These vibrations are attributed to a three-lobed bit pattern — or an n-lobed pattern — at the face of the rock being drilled (Figure 7). The bouncing-excitation condition is analyzed by Yang (1990). A lobed pattern occurs at the bottom (Figure 7a), with excavated spots (cams on bottom) corresponding to the shape of the cone bit. Skaugen (1987) shows an example in which a six-lobed pattern is produced by a tricone bit. If a lobed pattern is formed, the bit bounces off the bottom when the axial velocity of the cone rotating in the lobed-bottom pattern is higher than the maximum falling velocity of the bit according to Hooke's law, which governs the vibrations of the drill string. Yang (1990) shows that the bit bounces off the bottom when the first critical frequency of the forced vibration has the value

$$f_{c_1} = \frac{l_c g}{\pi c_1 s_0}, \quad (6)$$

where l_c is the length of the compressed portion of the drill string below the drill-string neutral point (Adams and Charrier, 1985; Poletto et al., 2001), g is the acceleration of gravity, c_1 is the propagation velocity of the axial elastic wave in the drill string, and s_0 is the peak-to-peak displacement value of the regular lobed bottom. Since $c_1 = 5130$ m/s, g = 9.8 m/s^2, and $l_c \sim 100$ m, from equation 6 it follows that even small values of s_0 can cause bouncing off the bottom in practical drilling conditions.

The lobed pattern is a frequent condition and induces large variations in the weight on bit. Yang (1990) points out that

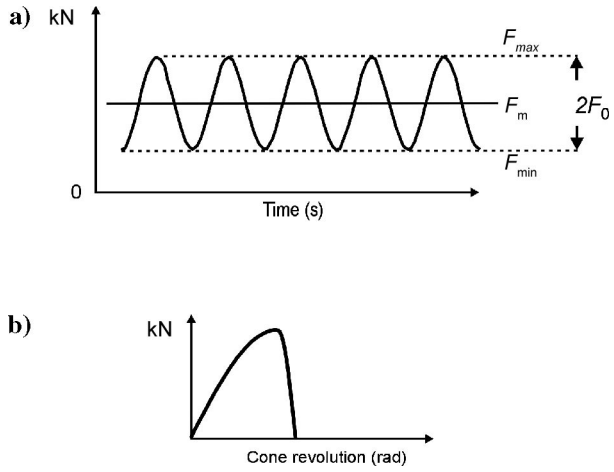

Figure 6. (a) Maximum $F_{\max}$, minimum $F_{\min}$, average F_m, and dynamic $2F_0$ forces. (b) Model of a single event of the indention force, with the unloading frequency five times higher than the loading frequency.

as long as a tricone bit keeps steady contact with the lobed bottom, the $2F_0$ peak-to-peak value of the downhole dynamic WOB cannot exceed the double static WOB (2 WOB). Hence, at the critical frequency of equation 6, we have (see Figure 7b)

$$F_0 = \text{WOB}. \tag{7}$$

Larger relative amplitude variations of weight and torque have been measured in real experiments with the bit bouncing off the bottom. Deily et al. (1968) show examples in which the bit weight varies from 0 to 625 kN when the nominal weight applied at the surface is about 180 kN and peak loads are more than 3.5 times higher than the load average values (Figure 7c).

Wolf et al. (1985) give a qualitative explanation of the feedback process linking drill-string dynamics with three-lobed pattern excitation. In this process, the dynamic response of the drill string forms the three-lobed pattern, which in turn provides excitation to the drill string. The force applied by the drill string to the formation, when in phase with the initial three-lobed pattern, deepens the three (n) low spots. Thus, excitation increases and resonances develop. The vibrations from a three-lobed pattern depend on the hardness of the formation and are larger for harder formations. Wolf et al. (1985) observe that this effect is excited, in general, at frequencies different from the natural resonant drill-string frequency (Dareing, 1982). After the maximum depth of the lobes that correspond to the geometry of the bit is reached, additional energy destroys the lobed pattern and the process decays abruptly. Skaugen (1987) observes that the minimum modulation period T_L, in which a multilobed pattern of maximum vertical amplitude a_L can be generated and broken down again (Figure 7d), must be greater than the time T_L necessary to drill the peak-to-peak lobe-pattern amplitude $2a_L$:

$$T_L = 3600\frac{2a_L}{\text{ROP}}. \tag{8}$$

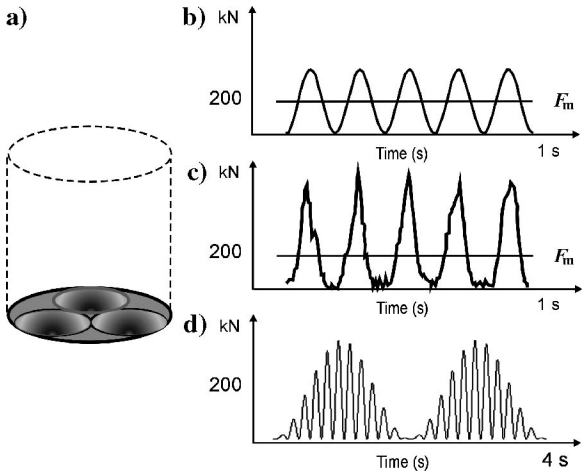

Figure 7. (a) Lobed drilling pattern with three spot cams. (b) Vibration model at the critical frequency (limit of bouncing off the bottom), where the average vertical force F_m equals F_0 and the maximum vertical force $F_{\max}$ equals $2F_0$. (c) Example of bouncing off the bottom; downhole real data. Modified after Deily et al. (1968). (d) Model of lobed-pattern modulation effect for periodic creation and destruction of the lobed bottom. Scale values are indicative of typical conditions.

For example, if ROP = 8 meters per hour (m/h) and a_L = 2 mm, we have T_L = 1.8 s. Here, we neglect any additional long-period precession effect because more work may be done on one side (front or back) of the pattern.

Analyses of SWD data demonstrate that three-lobed excitation makes an important contribution to SWD investigations. Figure 8 shows an example of good-quality axial-pilot and seismic vertical-geophone signals measured at the top of the drill string and at ground level for reverse vertical seismic profiling (VSP) purposes while drilling a carbonate formation using a tricone bit. The low-frequency peak at about 5 Hz in Figure 9 is interpreted as being from the three-lobed pattern excitation (using about 100 rpm), according to equation 5. Figure 10 shows the correlated SWD results versus offset. In general, drillers can consider large downhole vibrations either useful for increasing ROP or undesirable for their effects on wellbore stability and drill-string fatigue (Santos et al., 1999).

Hutchinson et al. (1995) have introduced a measurement while drilling (MWD) downhole assistant driller system prototype based on downhole measurements of forces and motion to detect undesired downhole vibrations, such as large-amplitude three-lobed patterns, in real time. This type of

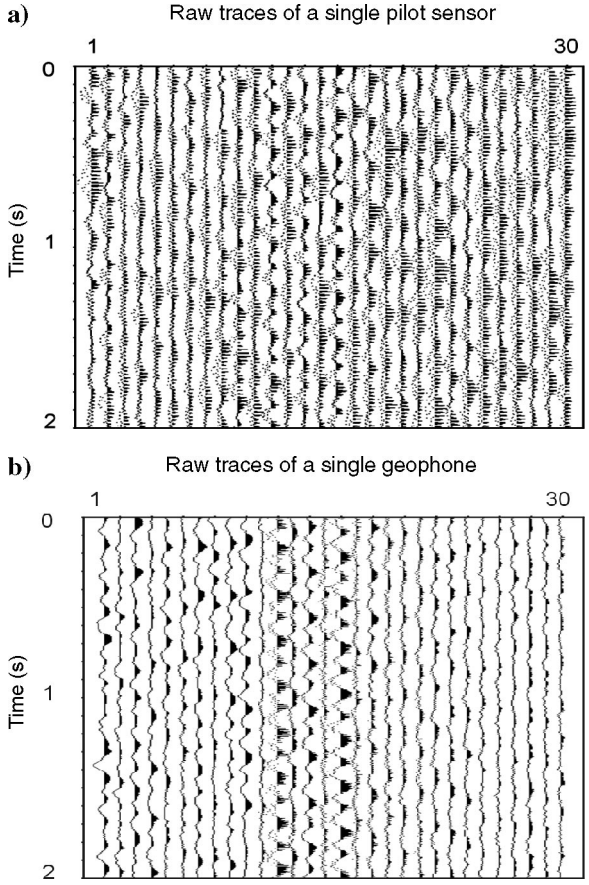

Figure 8. Drill-bit data measured while drilling with a roller-cone bit at 2140-m depth. (a) Traces of the axial pilot signal measured at the top of the drill string. The low-frequency component is interpreted as a result of the trilobe pattern. (b) Geophone signals measured at an offset of 450 m from the wellhead. The low-frequency lobed pattern is clearly detectable in the geophone data.

system can allow a driller to adjust the drilling control to remove undesired downhole effects and to improve drilling performance. In this case, a partial reduction of the SWD drill-bit signal can be expected.

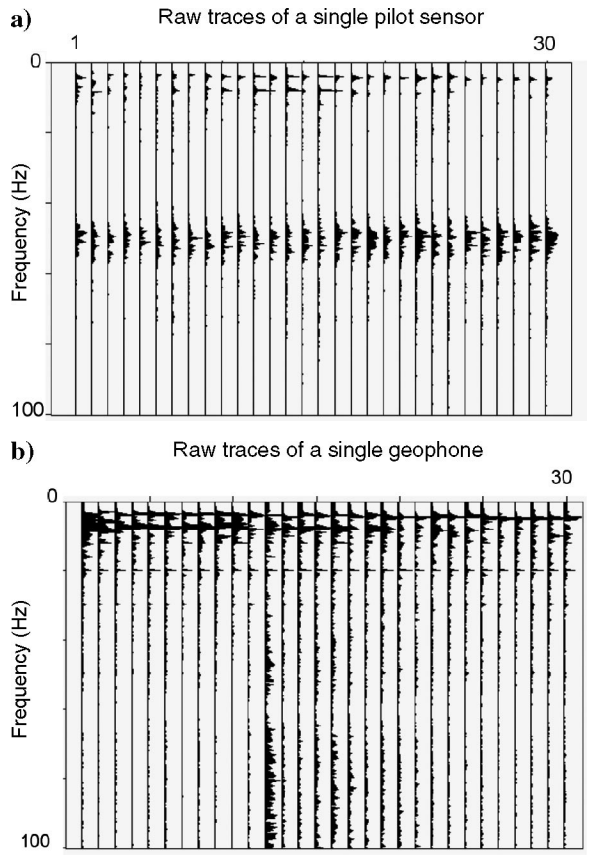

Figure 9. (a) Amplitude spectrum of the pilot traces of Figure 8. (b) Amplitude spectrum of geophone traces of Figure 8. The trilobed-pattern peak is clearly observable at 5 Hz frequency in both data sets.

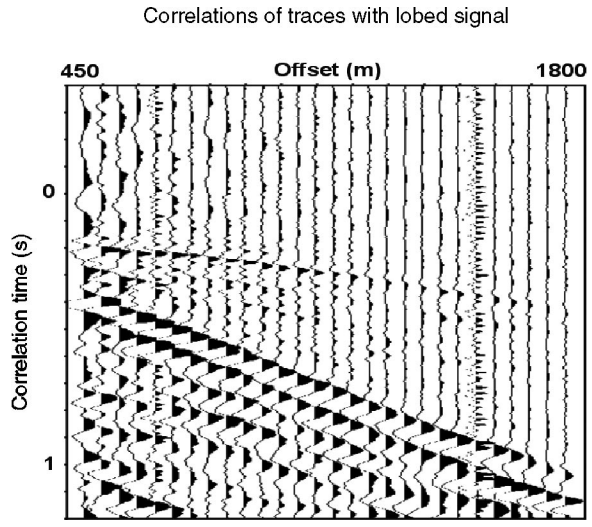

Figure 10. Correlations of SWD data versus offset. The pilot signal is deconvolved. Data are not bandpass filtered.

Effects of tooth wear on roller-cone vibrations

Roller-cone tooth wear, either milled steel or insert, is classified by levels of tooth wear from 0 to 8: zero corresponds to the status of a new tooth with no loss of tooth height and eight is the total loss of tooth height (Figure 11a) (McGehee et al., 1992b; Gabolde and Nguyen, 1999). Tooth wear produces two main effects for SWD. The first is a variation in the indention energy. The second is a variation in the row radius, which affects cone revolution speed and vibration frequency.

When the tooth wedge becomes dull and flat (a dull flat), a greater penetration threshold force is required. In the presence of wear, equation 1, relating force per unit chisel length and tooth-penetration depth, becomes

$$F(x_p) = \sigma_p(d_f + \tan\Theta x_p), \tag{9}$$

where d_f is the flat distance of the dull-bit wedge (Burgess and Lesso, 1985). As a consequence, the indention coefficient b_8 increases a little in the rotary energy equation 53 of part 1, while the gouging coefficient b_6 decreases significantly with increasing tooth flatness on account of wear. Falconer et al. (1988) calculate that the indention coefficient of the worn bit (b_8^{worn}) is always less than two times the coefficient of the new tooth (b_8^{new}), i.e., $b_8^{\text{worn}} < 2b_8^{\text{new}}$. This means that if we assume

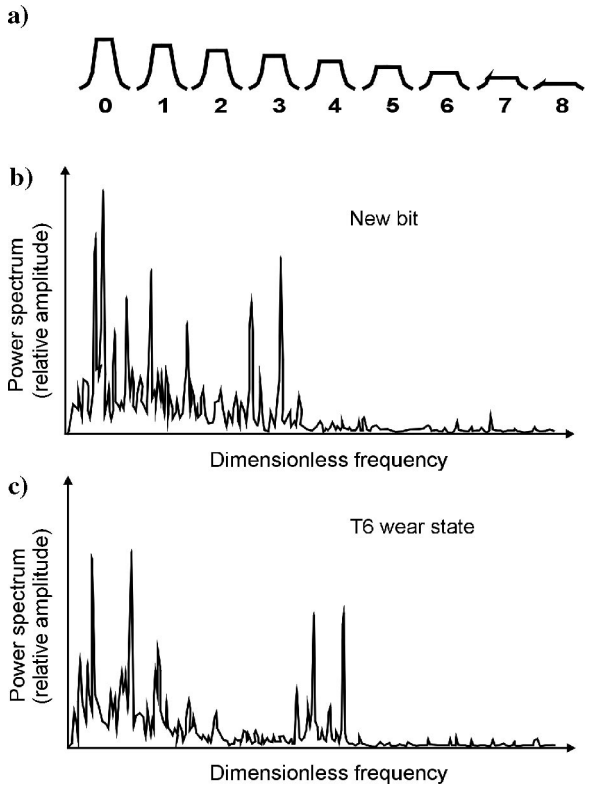

Figure 11. (a) Roller-cone tooth taper wear classification (modified after McGehee et al., 1992a). (b) Power spectra of a new (T0) and (c) worn (T6) roller-cone bit. Data are measured by using an atmospheric test machine. The frequency spectrum is normalized by the average bit-rotation speed and shows a wideband frequency content (with 120 rpm, this band could correspond to 100 Hz). Modified after Naganawa et al. (1995).

unit WOB, rpm, and bit diameter, the indention energy (dimensionless torque of equation 49, part 1) expended to drill at the same ROP (dimensionless ROP of equation 50, part 1) by a worn bit can be at most twice the indention energy expended by the new bit. Including the gouging term, wear typically results in decreased torque and increased specific energy E_S (equation 4, part 1) required to drill a unit volume of rock, rather than an increase in the average flux of energy radiated from the downhole vertical force.

Sheppard and Lesage (1988) measure the load distribution at the inner and outer rows of a new (T0 wear state) and worn (T3, i.e., 3/8 of the T-taper wear state) bit cone in laboratory experiments. They observe that load-on-row distribution is insensitive to lithology type but sensitive to wear geometry. With a new bit, a total load of 8 kN is distributed as 6 kN and 2 kN on the outer and inner rows, respectively. With the bit in the T3 wear state, the same total load is distributed as 5 and 3 kN on the outer and inner rows. In this wear state, the ratio of outer over inner loads changes from 3 to 1.66, thus modifying the frequency content of the total loading force and radiation properties.

The geometry of a worn bit also changes the cone-revolution frequency and the row vibrations. In fact, at a fixed rate around the bit axis, the cone revolution speed around the journal bearing axis increases as the wear progressively reduces the cone radius. Jardine et al. (1990) study the power spectra of the near-bit force and acceleration to determine the row-wear state from the bit signature. This method is based on the cepstral analysis of frequency peaks in data sampled as a function of the angle of cycles per cone revolution. These researchers observe that in the T3 wear state of a 29-tooth cone, the reduction in tooth-row radii increases the cone-speed factor. The cone-speed factor f_{cs} is the ratio of the cone-over-bit revolution speed; it typically varies from 1.25 to 1.30. It assumes values of 1.6 to 1.7 for bits with high wear (T8), with an approximately linear increment of the cone-speed factor versus wear. The cone revolution frequency can be approximated as

$$\omega_{\text{cone}} = \frac{2\pi\,\text{rpm}}{60}\left[f_{cs0} + (f_{cs8} - f_{cs0})\frac{j_w}{8}\right], \qquad (10)$$

where $f_{cs0} \sim 1.2$ and $f_{cs8} \sim 1.65$ and where j_w is the wear integer index (from 0 to 8). However, the calculation of the frequency spectrum of a bit row may be more complex for a worn bit than for a new bit because the wear state may introduce teeth irregularities. In this case, low-frequency harmonics of the cone speed, arising from the general periodic nature of the signal, become dominant peaks (Jardine et al., 1990).

ROLLER-CONE BIT AS A WIDEBAND SEISMIC SOURCE

As a basic requirement, a seismic source needs to be wideband (generally, two or three octaves are required). This is a necessary condition for obtaining short wavelets in time, by using either impulsive or nonimpulsive sources and coherency processing (i.e., as with vibroseis data). Thus, a basic condition for SWD is that the rotating drill bit produces wideband signals. Two factors contribute to making the roller-cone bit a wideband source.

Unevenness of formation and random breakage process

Drill bits, either roller cone or PDC, act by imparting a series of pulses to the rock. Laboratory tests performed by Sheppard and Lesage (1988) show that the frequency of the pulses produced by the periodic loading and unloading of the indentor teeth can be related to the roller-cone revolution speed and geometry. Hardage (1992), using the results of Sheppard and Lesage (1988) to analyze the vibrations produced by the roller-cone bit as a percussive source, proposes that each tooth pulse can be considered — at least ideally — as a wideband signal, which ultimately contributes to making the spectrum of the resulting SWD signal wideband. Ma and Azar (1985) and Ma et al. (1995) analyze the dynamic model of roller-cone bits and observe that the interacting action of the teeth in contact with the bottom-hole formation varies with time and can be regarded as a random stable process. Ma and Azar (1985) observe that the angular speed of the cones and bit can be considered an ergodic stationary process — with positive or negative speed variations corresponding to the depth transition steps of Figure 3 — and that the tangential tooth speed is random because of the slippage of the contacting teeth as a result of gouging and scraping effects, especially in medium and soft formations.

Bandwidth amplification by vibration-mode coupling

Periodic force components are a source of forced excitations for bit axial vibrations. Axial vibrations are caused by teeth indention, the bottom-hole lobed pattern, and mud-pressure modulation. However, downhole measurements of forces and acceleration show that axial and rotational vibrations at the bit have large quasi-random components (Skaugen, 1987). These are attributed to the unevenness of the formation strength and random breakage process and also to amplification by vibration mode coupling. In fact, the downhole rate of drill-bit rotation is often far from uniform because of large torsional drill-pipe flexibility (Hasley et al., 1986; Skaugen, 1987) and the torsional modes interacting with the forced axial vibrations of the drill string. As a result, the spectrum of the excitation modes becomes wideband.

In some cases, the torsional rotations (fundamental or pendulum and higher torsional modes) can be large enough to produce periodic stops in the downhole bit rotation (see Appendix A). As the top of the drill string keeps rotating, the string is wound up and energy is stored in the string, which acts as a torsional spring. Then, at increasing torque, this elastic energy is released, the bit starts spinning, and its speed increases and then slows down and stops again in a periodic winding and unwinding process. Jansen et al. (1995) show examples of downhole rotation speed with periodic zero-speed intervals and peaks six times higher than the surface average rpm value (Figure 12). In this process, there is a difference between static and dynamic friction, so that torque fluctuations do not damp out during sliding and more torque is required to remove the static condition of no rotation. This explains why aggressive bits, such as PDC bits (see next section) more than roller-cone bits, in some cases tend to produce the so-called stick-slip phenomenon, which accelerates bit fatigue. Chen et al. (1999) observe stick-slip events in roller-cone bit data acquired downhole by an instrumented tool in a 2000-m

full-scale well test. Stick-slip did not adversely affect ROP, and during slip, WOB increased from 35.6 to 93.5 kN while torque on bit changed from 0.27 to 1.1 kNm. In real drilling situations, the frictional interaction between drill string and wellbore also results in torque transfer to the drill string of a more stochastic nature.

PDC BIT

PDC bits (trade name Stratapax) were introduced in the early 1970s and have widely replaced roller-cone bits for drilling in soft and nonabrasive formations and, in part, in hard formations (Brett et al., 1990). The PDC bit has no moving parts and longer drilling life; thus, its use reduces cost (Figure 13). This type of bit is designed to drill by a cutting, shearing, and grinding action using chisels (sintered diamond cutters), which are fixed inserts set directly in its tungsten carbide body. The rake angle of a cutter is the angle made by the front of the cutter with the direction of impact (Figure 14a). Some types of cutters self-sharpen while drilling.

The PDC body can be formed with blades — regularly or irregularly spaced — or with a flat body. The distribution and the dimension of the cutters, either on the blades or on the body, are very important for assessing the effective and stable drilling action of PDC bits, which perform very well in soft formations but may have more stability problems and limitations in hard or abrasive formations where severe vibrations with high-impact loadings and wear may quickly destroy the bit (Langeveld, 1992a). Like roller-cone bits, PDC bits have jet nozzles to eject the mud that washes cuttings away from the bit face.

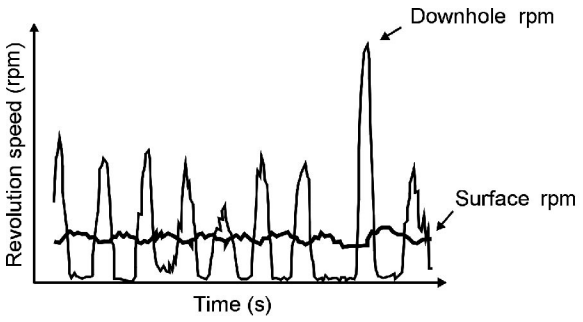

Figure 12. The downhole rotation speed has large fluctuations and stops (stick-slip), while surface rpm remains nearly constant. Modified after Jansen et al. (1995).

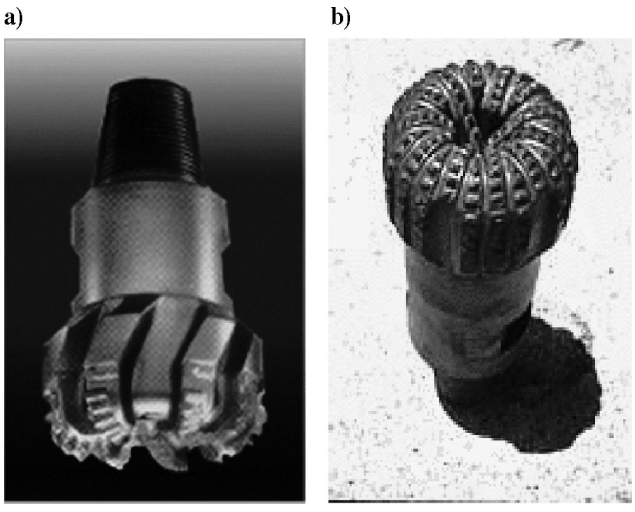

Figure 13. (a) PDC bit. These bits are used successfully in soft-medium nonabrasive formations. (b) Diamond bit usable in harder formations.

PDC BIT AS A VIBRATION SOURCE

The working load, or WOB, used for PDC bits is typically lower (e.g., 20–40 kN) than the load used with roller bits, so drill-string fatigue from vibrations is significantly reduced. In fact, PDC bits act primarily as shearing tools; in general, they produce poorer SWD axial pilot signals and compressional vibrations than do tricone bits, which use both gouging and percussive action. For instance, Falconer et al. (1988) assume that for PDC bits there is no energy term associated with the penetrating action of the teeth in the rotary drilling equation 53 of part 1, so that

$$b_{8\,\mathrm{PDC}} \cong 0. \tag{11}$$

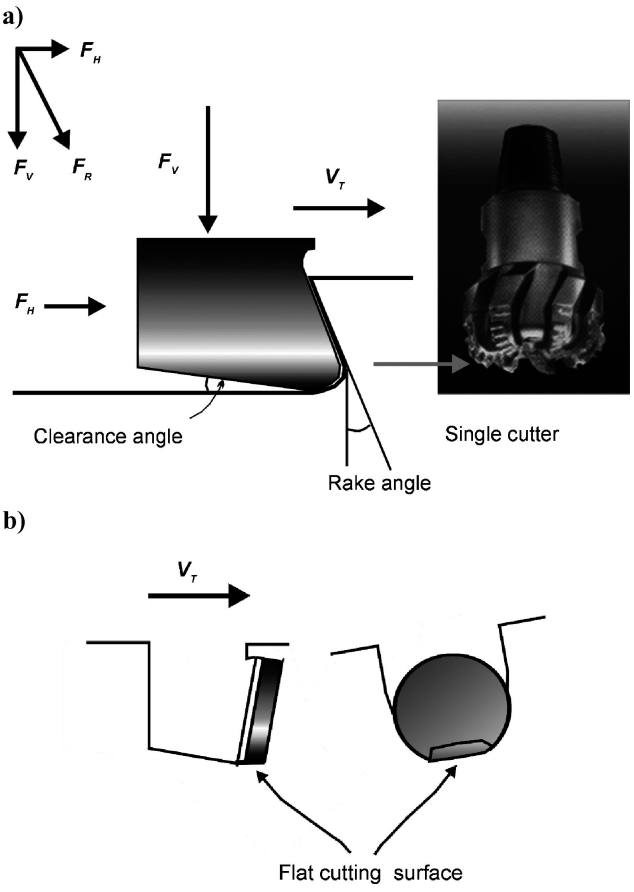

Figure 14. (a) Vertical F_V and horizontal F_H forces of a single cutter; F_R is the resultant force from a composition of F_V and F_H. With the presence of side lateral forces, the F_p and F_d penetration and drag forces are used instead of F_V and F_H. Modified after Duc et al. (1972). (b) Wear-flat area of a cutting. The penetrating force is directly proportional to the wear-flat area. Modified after Glowka (1986).

These authors use

$$b_{6\,\mathrm{PDC}} \cong 0.25. \tag{12}$$

Because there is no mechanical action associated with tooth vertical penetration in the PDC rotary-drilling process, the contribution of axial vibrations for SWD purposes is reduced and is more difficult to quantify. However, vertical and lateral forces are produced by the impact of the individual PDC cutters and vibrations of the PDC bit/drill-string system. In addition to the disadvantage of generating poor seismic signal excitation, PDC bits are commonly used jointly with downhole motors or turbines, which produce additional less-favorable conditions for SWD investigations. As a large (and increasing) number of wells are drilled with this assembly, effective use of SWD beyond roller-bit drilling is an important aspect that can be solved by multichannel processing and downhole near-bit measurements of PDC axial vibrations (Poletto et al., 1997).

Analysis of PDC single-cutter forces

The stress concentration induced in elastic rocks under a diamond-bit tooth during the working process of drag-bit blades is studied by Duc et al. (1972). They analyze, in bench tests, the plane-stress conditions produced in the rock by a tooth subjected to the effect of the vertical force F_V produced by the load on bit and the horizontal force F_H created by the applied torque (Figure 14). Their analysis extends to the fracture initiation state in the vicinity of the contact area as a function of loading by assuming the fracture model on the basis of the Griffith-Walsh criterion. The effects of the two fundamental mechanisms, cutting and grinding, are analyzed.

In the cutting mechanism, high-compression stress concentrations are induced under the tooth for clearance angles other than zero (Figure 14). Duc et al. (1972) observe that the stress transmitted by the diamond bit can be represented by an inclined force in the model [they consider examples with applied forces $F_H = (1/2)F_V$]. At the same time, high tensile stresses appear around the cutting edge.

In the grinding mechanism, tensile stress appears behind the tooth, and high compression stresses are propagated in front of it. In the grinding mode, friction increases tooth efficiency.

Glowka (1986) develops a fairly exhaustive study of laboratory experimental data and a method based on a single-cutter analysis for predicting cutter forces, temperature, and wear on PDC as well as integrated bit-performance parameters such as WOB, torque, and bit imbalance. Imbalance is defined as the ratio of total side force over WOB. Glowka's analysis reaches the important conclusion that the single penetrating force of a worn cutter for a given depth of cut is directly proportional to the wear-flat (flat cutting surface) area of contact between worn cutter and rock (Figure 14b). As an example, for a given cutting depth, sharp cutters correspond to low penetrating forces, e.g., 2.2 kN, while worn cutters correspond to high penetrating forces, e.g., 11 kN.

Direction of single-cutter force. — Transverse forces are related to vertical forces as follows: The cutter drag force F_d is proportional to the penetrating force F_p (corresponding to F_H and F_V in Figure 14a). Glowka (1986) defines the cutter drag coefficient as

$$\nu_d = \frac{F_d}{F_p}. \tag{13}$$

The drag coefficient ν_d (hence, the direction of the resulting force) is a function of rock type and is relatively independent of the depth of cut and wear-flat area. Values of $\nu_d \sim 0.65$ and $\nu_d \sim 0.95$ in dry tests with granite and sandstone samples, respectively, are estimated. In water-drilling (mud) conditions at elevated nozzle pressures, the penetrating stresses are significantly reduced (Glowka, 1986) by the effects of hydraulic horsepower on PDC bit ROP (Holster and Kipp, 1984). With jet pressures of 13.8 MPa, the penetrating stresses required to cut a given depth of granite are reduced by 10 to 15% with respect to the presence of water. With assistance from 31-MPa water jets, cutter penetrating stresses are reduced by 50 to 65% (a 31-MPa jet causes considerable damage to a rock surface). Drag forces are reduced by the presence of water but are not greatly affected by jet pressure.

PDC bits with different profiles and cutters loaded vertically by WOB and laterally by side forces have different distributions of forces. The total WOB is the sum of the longitudinal components. The drill-bit torque is the sum of the moments caused by the circumferential drag forces.

Influence of wear on performance parameters. — Wear greatly affects bit performance. Higher WOB is required for drilling with a worn bit at the same ROP as a sharp bit. For instance, to drill with a sharp bit at an ROP of 9 m/hour a 16-kN WOB may be required, whereas about ten times this WOB may be required for drilling at the same ROP with a worn bit. Furthermore, excessive drilling torque is an indicator of bit-wear conditions. Wear conditions may affect balanced drilling and cause large lateral vibrations (stick-slip). To avoid high, nonuniform wear conditions, the density of the radial distribution of cutters and the effects of the bit profile are very important parameters to consider.

Influence of downhole pressure on cutter forces. — Other downhole conditions influencing PDC cutting action are formation and mud pressure. PDC normal (penetration) and drag forces on single cutters are studied by Zijsling (1987), who simulates downhole pore and total bottom-hole pressures. In a laboratory, he uses a single-cutter testing system and shale samples to study different simulated pressure conditions that govern the cutting process at different drilling depths. Zijsling reports the effects of pressures on dynamic PDC forces varying from about 3 to 30 kN on individual cutters at several simulated drilling depths from 800 to 3500 m. He shows that the dilatancy of the rocks is responsible for this behavior.

Dynamic variation of PDC cutter forces

Behr et al. (1993) have developed a 3D PDC model to evaluate cutter loading in inhomogeneous rock drilling and in cases where the bit whirls laterally. In this model, the WOB, torque, and bit imbalance forces are updated each time an individual cutter force is modified. The following cases of high drilling loads are studied by model and laboratory tests.

Tilted-bed boundaries. — Drilling tests evaluated the performance of different PDC bits drilling across a tilted-bed boundary between shale and limestone. Behr et al. (1993) report that at a constant 22-kN WOB, the load on the cutters remains nearly the same (the range of variation is not specified) when drilling only 100% pure shale or limestone. But when drilling across the bed boundary, the load on individual cutters varies greatly within a revolution — from about 1.2 kN to about 8.5 kN — because cutters alternately engage in shale or limestone. In other examples, both vibration and downdip displacement of bits with long tapered profiles are observed.

Drilling nodules. — When the formation is inhomogeneous, larger PDC vibrations may occur. An example is soft-medium shale containing much stronger nodules (concretions), which are formed when calcite solution deposits in the pores. The dimension of these hard nodules may be about a foot. Simulation drilling tests by Behr et al. (1993) were run under constant WOB of 44.5 kN using a four-blade PDC bit. The normal load on a single cutter was about 2.7 kN, while the peak force on the cutter from the increase in load during engagement with the concretion was about 26 kN. In this case, the vertical force on the cutter was about 18 kN, i.e., 40% of the total load. An approximately tenfold increase in the imbalance lateral force (passing from about 3.5 to 38 kN) was also measured. This force might produce whirl.

Whirling bits. — As may happen with roller-cone bits, PDC bits may produce lobed-bottom patterns that may cause severe vibrations. In this case, the lobed patterns are related to the lateral motion of the center of rotation of the bit, which precesses out of the bit axis and whirls (Brett et al., 1990). Behr et al. (1993) observe in the laboratory the lobed-bottom precession of a four-blade bit that forms a nine-lobed, star-shaped borehole wall instead of a cylindrical one. High imbalance and normal single-cutter forces with large variations and a periodicity of about eight cycles per revolution of the drill string are reported. For a bit with equally spaced blades, assuming whirl frequency per revolution f_w, the number of lobes should be

$$N_{\text{lobe}} = (f_w + 1)m, \qquad m = 1, 2, 3, \cdots. \tag{14}$$

Bit precession causes intermittent contact between the cutters and the lobed-shaped formation; as a consequence, the normal (i.e., perpendicular to the cutter motion) tooth force varies. Examples of normal forces on a single tooth are about 0.5 kN during steady-state drilling without whirling, to about zero during whirling when the tooth is off the bottom, and up to about 5.8 kN when the tooth is fully engaged with a formation lobe. The WOB resulting from the sum of all the single-tooth vertical forces oscillates around a mean value of 22 kN. Periodic (with eight cycles per drill-string revolution) imbalance forces range from 3.5 to 11.1 kN, and the centrifugal force is about 4.7 kN. The design of antiwhirl bits, introduced in the early 1990s, is based on the concept that the cutter is placed on the bit to obtain a nonzero side force (Cooley et al., 1992; Hanson and Hansen, 1995). This side force stabilizes the bit against the wall of the well so the instantaneous center of rotation of the PDC remains at a fixed position.

Dynamic models of PDC-bit axial vibrations

The lateral, torsional, and axial vibration modes of a PDC bit are calculated by Langeveld (1992b), who develops a 3D, fully dynamic PDC-bit and drill-string numerical model, including formation removal. To calculate the vertical component of the time-varying force resulting from the cutting action of the bit, the drill string is modeled as a damped mass-spring system by the axial equation of motion. The following dynamic results are reported by Langeveld (1992b) using 2350 m of 5-in. drill pipe, 150 m of $6\frac{1}{2}$-in. drill collars, and three different $8\frac{1}{2}$-in. antiwhirl PDC bits. Axial vibrations occur from 4 to 7 Hz (in relation to rapid fluctuations of the ROP). This axial response is governed by both the drill-string properties and the properties of the formation. Langeveld (1992a) concludes that PDC bits may induce large axial drill-string vibrations during transients in the applied load (WOB). However, the effect of the overall axial response on the bit/drill-string system is small, and sensitivity analysis indicates that major amplitude vibrations in the reactive force of the drill string occur at relatively low WOB and high rotary speeds.

Based on Langeveld's model and results, Hanson and Hansen (1995) have developed a numerical bit-dynamics method to predict PDC-bit performance under the conditions of a full-scale drilling simulator test. They test 20 bit designs of different diameters of both conventional and antiwhirl types. Normal (perpendicular to the direction of the cutter motion) and tangential (in the direction of the cutter motion) single-cutter force models are calculated. This dynamic analysis shows the presence of large vertical rock vibrations during the whirling state, with load variations on the order of 44.5 kN. As the vertical load increases and the ROP reaches the transition ROP value of 14.6 m/hour, the axial vibrations diminish and drilling stabilizes. After stabilization, some low axial vibrations still persist. The spectra of the vertical vibrations (WOP) are computed at ROPs of 7.3 and 14.6 m/hour and 120 rpm. They show a large bandwidth feature from 0 to 80 Hz. In particular, when an eight-blade bit whirls, a peak at 16 Hz clearly occurs, and a consistent nine-lobed pattern is observed. On the other hand, the same analysis performed using conventional bits gives examples that never stabilize.

BIT VIBRATIONS INDUCED BY MUD-PRESSURE MODULATION

Another axial force exciting axial vibrations is the pulsation from mud-pump pressure fluctuation. For double-acting pump cycles, the fluctuation frequency equals four times the cycles per minute. Typical values of strokes (or cycles) per minute (SPM) are from 60 to 70. Because a number N_P of two to four pumps can be used simultaneously, the total frequency is (if we assume the pumps are alternated with a synchronized phase), in hertz,

$$f_{\text{pump}} = 4\frac{\text{SPM}}{60} \times N_{\text{P}}, \tag{15}$$

typically 8–16 Hz. Cunningham (1968) shows examples of a moderate weight fluctuation of about 67 kN, corresponding to a pump-pressure fluctuation of about 4150 kPa.

The importance of the pressure fluctuation on the bit weight can be appreciated by assuming a static drill stem held rigid at both ends with a pulsating pressure inside. With no axial

motion of the drill stem at any point, the weight fluctuation of the bit resulting from 6900 kPa pump-pressure fluctuation could be 29 kN for a $5\frac{1}{2}$-in. drill pipe (Cunningham, 1968). Deily et al. (1968) analyze the balance of the forces produced by the fluid pressure acting at the bit and directed along the axis of the tool. Assuming the jet-reaction force attributable to mud injection through the jet nozzles is small, they give the following equation:

$$f_T = F_P + p_o \Delta A_o + p_i \Delta A_i, \tag{16}$$

where f_T is the reaction force in the tool, $(p_i \Delta A_i)$ is the force produced by the inside pressure, $(p_o \Delta A_o)$ is the force produced by the outside pressure, and F_P is the axial force in the pipe directly below the tool (Figure 15). To calculate the magnitude of the pressure effects, Deily et al. (1968) assume $p_i =$ 24 000 kPa and $p_o = 14\,150$ kPa. Because the inner and outer sections of the tool are roughly 100 cm^2 in surface area, these authors obtain a force induced by the differential pressure effect of 270 kN, which is comparable to load-on-bit values and must be subtracted from the bit-weight recordings. This effect is strictly related to the geometry of the downhole tools and string.

NUMERICAL EXAMPLES OF DRILL-BIT VIBRATIONS

The following calculations of the radiated energy are performed by considering periodic bit vibrations. As discussed in part 1, random effects in real drilling conditions may introduce sudden variations in signal amplitude and phase, which could increase the amount of radiated energy (part 1). For this reason, the values calculated in the following numerical examples must be considered as lower limits for the energy radiated by the working bit at the given drilling and geological conditions.

Radiation caused by teeth vibration

A peak-to-peak periodic vertical force of about 16 kN is measured by Sheppard and Lesage (1988) for the 19-tooth outer row of a single cone. Rotation speed is not specified. If we assume 60 rpm as a reference value and consider only this row, the pulsation is $\omega_{\text{row}} = 2\,\pi \times 19 \times 1.25 \approx 150$, where 1.25 represents the average cone-to-bit revolution ratio. Rock is assumed to be a Poisson's medium with Young's modulus $Y = 40$ GPa and density $\rho = 2400$ kg/m^3. The integrated radiation impedance of equation 27 (part 1) is, in kilograms per second,

$$\mathcal{Z}_R^{(P)} \approx \frac{1}{0.302} \frac{\rho \alpha^3}{\omega_{\text{row}}^2} \approx 3.15 \times 10^{10}. \tag{17}$$

The radiated power of equation 26 (part 1) is calculated by assuming that the dynamic force F_0 equals 0.5 times the peak-to-peak load force (see equation 4), i.e., $F_0 = 16/2$ kN, which gives the power flux, in watts,

$$W_R^{(1\text{cone})} \approx \frac{8000^2}{2} \frac{3}{3.15 \times 10^{10}} \approx 3 \times 10^{-3}, \tag{18}$$

where the factor three is introduced to account for the average effect in loading and faster unloading. So, the energy radiated by the outer row in one hour of continuous drilling during the single-cone test is 11 J. If we assume that the load is distributed equally on all cones and that the teeth in contact with rock are in phase, we can substitute the total downhole load force to the single-row load. The analysis of downhole data shows that the magnitude of the total loading during full-scale drilling can be on the order of the surface WOB. This force can be assumed to be much higher than the laboratory value of 16 kN (e.g., 240 kN), and the rpm frequency can be doubled (rpm = 120). If we assume that total and dynamic loads are comparable, then values of the energy radiated for teeth indention are about 900 times higher than those of the experiment discussed above. We obtain an energy on the order of 10 kJ per drilling hour (i.e., 2.8 W). This value is calculated assuming a Poisson's medium and increases to about 29 kJ/hour (i.e., 8 W) if the rock's Young's modulus is Y = 20 GPa. Since most of the energy is radiated in the form of shear waves, by using equations 22 and 24 of part 1, we can show that, for a given P-wave velocity, the amount of radiated energy is very sensitive to (α/β) — i.e., to the V_P/V_S ratio. Figure 16 shows the energy variation with V_P/V_S ranging between 1.2 and 2.4. This effect also changes the global impedance at the bit, given for a Poisson's medium, by equation 48 of part 1.

Radiation caused by trilobed vibration

Let us consider a bottom-hole lobe pattern in its critical condition given by equation 6, after which the bit bounces off the bottom. In this case, peak-to-peak force equals 2WOB, $F_0 =$ WOB, and $\omega_{\text{L}} = 3 \times 2\pi$ rpm/60 s^{-1} $\sim$ 38. Using WOB = 240 kN, rpm = 120, $Y = 20$ GPa, and $\rho = 2400$ kg/m^3, we obtain $W_R \sim 0.17$ W. The low-frequency lobe-pattern energy radiated in one hour of drilling is about 600 J. Note that in this case, I have not used any factor of energy amplification to account for sharpness of the loading curve as I did for teeth loading and unloading (factor of 3), even if lobed vibrations appear to be very sharp in many plots of downhole measurements

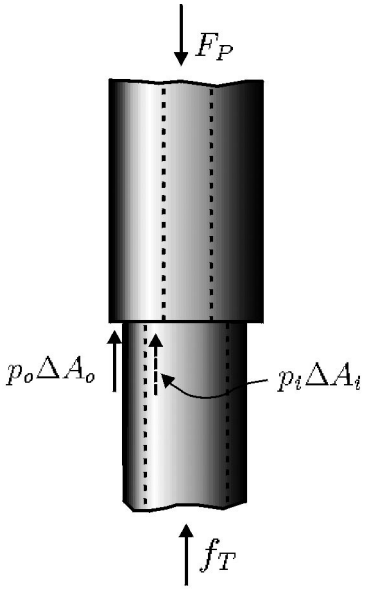

Figure 15. Model used to calculate the modulation of the axial force by mud pressure. The mud forces depend on downhole tool and drill-string geometry.

reported in drilling literature. When drill-string torsional, fundamental vibration modes induce frequency modulation, this energy value can be about 1.5 times higher, i.e., about 1 kJ. This value increases if we consider the condition of the bit bouncing off the bottom (e.g., with $2F_0 = 3$ or 3.5 WOB).

Composite vibrations

Assume that the cone-row rotation speeds are not equal and the rock contacts of the indentor teeth are not in phase in the three cones. Assuming $F_{\min} = 0$ in equations 2–4, we can write

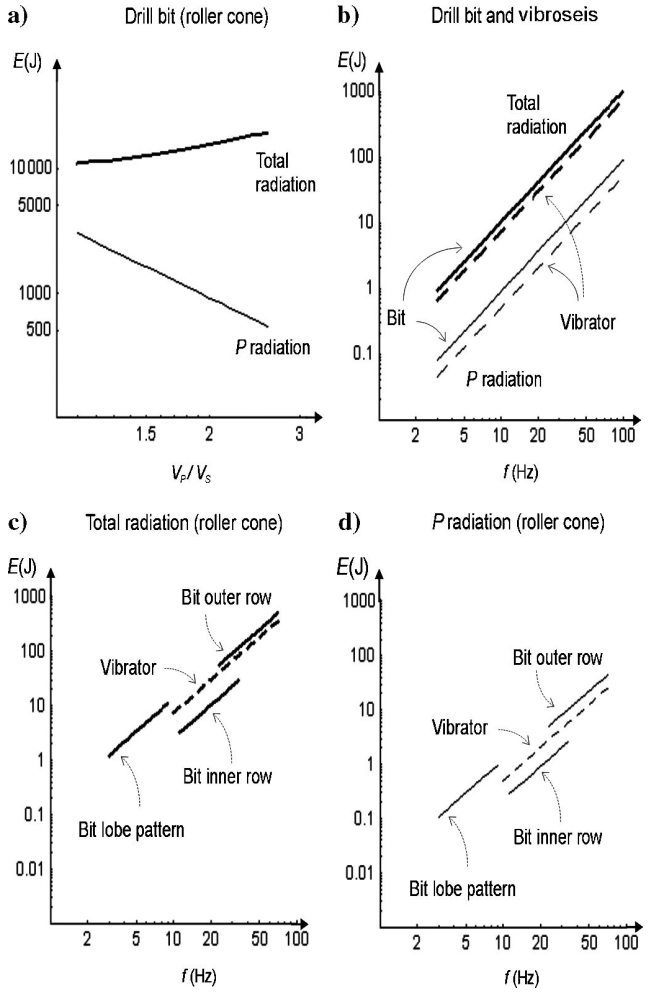

Figure 16. (a) Amount of energy radiated in 1 hour by an ideal 19-tooth row, represented versus V_P/V_S ratio. (b) Comparison between powers of a conventional surface vibrator (energy in 1 min; dashed lines) and roller-cone drill-bit source (energy in 30 min; continuous line) at different frequencies from 3 to 100 Hz (the calculation includes the lobe pattern, 9-tooth inner and 19-tooth outer-row vibrations). A total bit vertical load of 240 kN (160 kN on outer and 80 kN on inner rows), 120 rpm, cone rotation factor of 1.25, Poisson's formation of Young's modulus of 20 GPa, density of 2400 kg/m^3, and two vibrators of 61,000 lb are assumed. (c) Total power (energy in 30 min) radiated from 19-tooth outer, 9-tooth inner rows and lobed–pattern forces (continuous line) are compared separately (for $60 \le$ rpm ≤ 120 rpm) to the radiation from two vibrators (energy in 1 min, frequency from 16 to 70 Hz). (d) Compressional power calculated as in (c).

the force as

$$F(t) = \sum_i F_i[1 + \sin(\omega_i t + \phi_i)], \tag{19}$$

where F_i and ϕ_i are loads distributed on the cone rows and random rotation phases [e.g., for slippage effects (Ma et al., 1995)], respectively. We can use equation 29 (part 1) to calculate the radiated energy. If we assume that the different components are uncorrelated, we obtain $I_f = \frac{1}{2}\sum_i (F_i\omega_i)^2$. In the case where the load is distributed equally on the three cones, we have

$$W_R^{(3\,\text{cone})} = 0.151\frac{F_0^2}{3}\frac{\hat{\omega}^2}{\rho\alpha^3}, \tag{20}$$

where $\hat{\omega}^2 = 1/3\sum_{i=1}^{3}\omega_i^2$. As a rule of thumb, we may assume that the factor 1/3 in equation 20 is compensated by the factor three of loading-unloading effects. In this case, equation 20 can be rewritten as

$$W_R^{(3\,\text{cone})} \approx 0.151\frac{F_0^2\hat{\omega}^2}{\rho\alpha^3}, \tag{21}$$

and $W_R^{(3\,\text{cone})} \sim W_R^{(1\,\text{cone})}/3$, where $W_R^{(1\,\text{cone})}$ is given by equation 18 of the single cone. Contrarily, if the cones rotate in phase, we again have the results obtained with the single cone.

Vibrations modulated in amplitude

Modulation effects can be introduced by lobe-pattern forces, mud-pressure fluctuations, or drill-string resonances. Let the modulation of a row force of equation 2 be expressed by a function of the type

$$F(t) = (F_m + F_0 \sin\omega_{row}t)\,(1 + \sin\omega_{mod}t)\,. \tag{22}$$

The row force modulated by the lobe pattern produces an amount of radiated energy 1.5 times that of the unmodulated row force.

Roller-cone tooth wear

Sheppard and Lesage (1988) show that the geometry of the worn bit changes load distribution. In worn bits, the total load is more equally balanced between the outer and inner rows, while in a new cone, the load is greater on the outer row. Even if the total load is unchanged, these examples do not report the changes in the dynamic loads produced by the shorter dull teeth, which may be of minor magnitude with the same total load. Furthermore, any uneven wear introduces low-frequency harmonics, so the spectrum of vibrations is redistributed on a lower frequency band. Despite a possible small increase in the cone revolution speed factor, all previous effects lower the amount of radiated energy. The fact that a higher indention coefficient (b_8) is calculated in the rotary drilling equation 53 of part 1 is only an apparent contradiction. In fact, we can expect worn bits to drill more slowly and more seismic energy to be obtainable by prorating the listening during the longer times used to drill the same depth interval.

Vertical vibrations calculated by rotary drilling equation

I have used rotary drilling equation 54 of part 1 to relate drilling and radiation energies. This approach requires calculating the phase factor $\cos\varphi$ between the force and velocity at the bit and knowing the bit constant b_8, which is reported in the literature only for milled roller bits. Assuming a constant bit parameter, this equation could be used to estimate relative variations in intervals drilled with the same bit.

Estimation of radiated power from axial drill-string vibrations

The best way to calculate the radiation performance of the drill-bit source is to measure vibrations downhole near the bit. The force data, related to acceleration by equation C-4 of part 1, are derived with respect to time and are squared to calculate I_f of equation 29 (part 1). As an example, assume a pipe with drill collars that have outer and inner diameters of $8\frac{1}{2}$ and $2\frac{3}{4}$ in., respectively, and acceleration of 17 m/s^2 (1.7 g) at the only harmonic frequency of 30 Hz when drilling a formation with $Y = 20$ GPa and $\rho = 2400$ kg/m^3. Using equation C-5 of part 1, we obtain a radiated energy of 3.7 kJ during one hour of drilling.

RADIATION PROPERTIES OF CONVENTIONAL SOURCES

The total recording times used to acquire SWD data of a single depth level may vary from a few minutes to hours (Miranda et al., 1996). This long listening time of the power radiated while drilling makes it possible to obtain sufficient seismic energy. From previous calculations, it follows that the energy radiated by the drill-bit source in the rock during realistic SWD acquisition intervals can be compared to the working energy of conventional seismic sources, such as vibrators (mainly onshore) and air guns or water guns (onshore and offshore).

Vibroseis source

The seismic emission of mechanical vibrators depends on many factors, such as the frequency of the exerted force, ground properties, soil coupling, vibration plate deformation, and the use of vibrator arrays. Assuming a rigid plate (in which case the displacement of the soil particles at the contact of the plate equals the plate displacement), Cassand and Lavergne (1971) analyze the forces exerted by a single plate, multiple plates, coupling effects, and the displacement of ground particles at a great distance from the source. In ground with high radiation impedance (discussed in part 1 and defined as the ratio of applied force to particle velocity, reciprocal of admittance), i.e., hard rock, the force F_s exerted by the single plate practically equals the vibration generator force F_e. In rocks of low radiation impedance, i.e., loose ground, these forces are equal only at low frequencies, while deviation of F_s/F_e (which defines vibration coupling) at high frequencies depends on ground and plate properties and is a matter of proper design acquisition by vibrators (the applied ground force is available if a ground-force phase-locking system is used).

Single vertical vibrator

Radiation analysis is based on results of Miller and Pursey (1954), who calculate the power transmitted by a single pulsating plate into a semi-infinite, elastic, homogeneous, isotropic medium with a Poisson's ratio 0.25. If $2F_s$ and ω are the peak-to-peak vertical force impressed on the ground and the angular frequency of the pulsation, respectively, the following power distributions are obtained:

$$W_\alpha^{\text{vibro}} = \eta \frac{\omega^2 F_s^2}{4\pi\rho\alpha^3}, \tag{23}$$

where $\eta = 0.333$, 1.246, 3.257, and 4.836 for compressional, shear, surface, and totally radiated waves, respectively. Hence, approximately 7%, 26%, and 67% of the power of a single pulsating plate are transmitted in the form of compressional, shear, and surface waves, respectively. The total energy of a sweep of amplitude $F_s(t)$ and instantaneous pulsation $\omega(t)$ is calculated by integrating $W_{\text{total}}^{\text{vibro}}(t)$ from zero to the sweep time length τ. Assuming F_s to be constant for a linear sweep varying from the initial to the final frequency ω_0 and ω_1, respectively, when the time t varies from 0 to τ, we have $\omega(t) = \omega_0 + (\omega_1 - \omega_0)t\tau^{-1}$. Assuming a slow frequency variation during interval τ (i.e., $\tau \gg 2\pi/\omega_{\min}$, where $\omega_{\min}$ is the minimum between ω_0 and ω_1), the total compressional energy can be calculated as

$$E_\alpha^{\text{vibro}} = 0.333\frac{F_s^2}{4\pi\rho\alpha^3}2\int_0^\tau \cos^2\left[\left(\omega_0 + \frac{\omega_1 - \omega_0}{2\tau}t\right)t\right]\omega^2(t)dt = 0.333\frac{F_s^2\hat{\omega}^2}{4\pi\rho\alpha^3}\tau, \tag{24}$$

where $\hat{\omega}^2 = [(\omega_1 - \omega_0)^2/3] + \omega_1\omega_0$.

Furthermore, the radiated energy in the vertical stack of correlations obtained with sweeps repeated more times in the same conditions is the sum of the energies of the individual sweeps. The compressional radiated power W_α^{vibro} of equation 23 in this paper is twice the compressional power W_r of equation 21 of part 1 radiated by an equivalent downhole bit force, in agreement with the heuristic consideration that double the energy is required to energize the entire space instead of a half-space. This relation is not true for the shear component, which is more affected by free surface effects when produced by a vertical vibrator. Note that the total power W_R^{surf} calculated for the same vibration conditions using Simon's equations for surface-impact loading processes equals the total power $W_{\text{total}}^{\text{vibro}}$ radiated from a single vertical vibrator (equation 23 with $\eta = 4.836$).

Array of vertical vibrators

In field applications, because of the weak amplitude of the emitted signal and the presence of environmental noise, arrangements of several pulsating plates (vibrator arrays) can be used simultaneously to reinforce the compressional signal at the expense of surface waves. In this case, the mutual admittances (impedances) of the plates vibrating in phase must be properly accounted for when calculating the radiated power. In fact, mutual effects are generated because the displacement under each individual vibrating plate is modified by the presence of the other vibrators (Cassand and Lavergne, 1971,

206–208). The effect is, at least ideally, that the power radiated by n closely spaced vibrators is approximately n^2 times the power radiated by a single vibrator. This fact could be accounted for by substituting a force of magnitude n times larger in equation 23. This approximation does not use a realistic boundary condition, and here it is a rule of thumb. Variation of radiated waves, baseplate properties, and vibrator spacing are discussed by Baeten and Ziolkowski (1990).

Table 1 shows an example of acquisition values used in a conventional VSP vibroseis application. The same formation of the numerical example in which the radiation from a 19-tooth single row was calculated is used. The total energy radiated by four vibrators energizing five repeated 12-s sweeps is 6.7 kJ. The compressional energy is 0.46 kJ.

Radiation from marine sources

Air guns, based on pressured bubble expansion, and water guns, producing waves by cavity collapsing, are used for offshore and onshore VSP surveying. Offshore, the guns are lowered into the water from the rig to acquire zero-offset VSPs or are towed by a vessel to acquire multioffset VSPs. Onshore, the guns are used in water-filled tanks dug near the well. Consider that in an ideal homogeneous, isotropic medium, a pressure-dilatation wave radiates with spherical geometry, with its power equally distributed and equal to its average value on the surface wavefront. On the other hand, the waves emitted by vertical forces produced by bits and vibrators have radiation lobes and, in the direction of the acting force have a maximum compressional power density three times their average compressional power density. The amount of energy effectively radiated depends on factors such as the energy of the source, bubble effects, water-pressure conditions, and loss of energy for the tank/formation reflection. The nominal energy of a gun E_{gun} is given by the product of its volume V_{gun} and working pressure p_{gun}, i.e., $E_{\text{gun}} = V_{\text{gun}} p_{\text{gun}}$. For instance, a gun of volume $V_{\text{gun}} = 400$ in.^{3} (0.00655 m^3) and of working pressure $p_{\text{gun}} = 2000$ psi (13 789 kPa) has a working energy $E_{\text{gun}} = 800\,000$ lb-force in. (90.4 kJ). A simple method for determining the relative potential energy of marine sources is to observe the bubble oscillation interval and measure the potential energy from a Rayleigh–Willis chart, which compares the energy of different sources (Dobrin, 1981).

Table 1. Example of conventional VSP vibroseis source.

Characteristic	Value
Number of vibrators	4
Peak force of single vibrator[1]	$2F_s = 61\,000$ lbf (271 kN)
Sweep length	12 s
Type of sweep	Linear
Start–end frequencies	10–70 Hz
Number of sweeps per level (vertical stack)	5
Formation's Young's modulus	20 GPa
Formation density	2400 kg/m^3
Formation's Poisson's ratio	0.25
Total radiated energy	6.7 kJ
P-wave radiated energy	0.46 kJ

[1]lbf = pounds force.

DISCUSSION OF RESULTS

I compare the calculated performance of the drill-bit source to those of vibroseis and air guns. Baeten and Ziolkowski (1990, p. 3) observe that vibrator sources (vibroseis) have some disadvantages compared with dynamite. They report a 2.5-kg dynamite charge can deliver about 10^7 J of energy, whereas a single vibrator delivers 1.2×10^6 J. To obtain sufficient energy, vibroseis units are typically used in arrays and with several sweeps in the same position. Table 1 calculates the radiation of an array of four conventional vibroseis sources used for VSP purposes. In this example, the total radiated energy is 6.7 kJ. The numerical examples calculated before for roller bits show that a comparable radiated energy (of about 10 kJ/hour) is obtained with 40 min of SWD listening by using a typical average row-cone frequency (see equation 22). Furthermore, radiation of the roller bit at low frequencies is much higher in the presence of a lobe-bottom-pattern vibration. The numerical calculations give (with no bouncing and including the pendulum effect; see Appendix A) a value of 1 kJ/hour, which is comparable to the total energy radiated at the same frequency by two vibrators in five repeated sweeps of 12 s.

To appreciate the comparable effects at the different frequencies, Figure 16 shows the compression power radiated by roller-cone bit and vibroseis sources in a bilogarithmic scale. In this representation, we can appreciate the linear trends of

$$\log W^{\text{vibro}} = 2\log\omega + \log\gamma_{\text{vibro}} \tag{25}$$

and

$$\log W_R = 2\log\omega + \log\gamma_{\text{bit}}, \tag{26}$$

where $\gamma_{\text{vibro}} = F_s^2/(12\pi\rho\alpha^3)$ and $\gamma_{\text{bit}} = F_0^2/(24\pi\rho\alpha^3)$ for vibrator and roller-bit sources, respectively. These calculations and the analysis of the wideband frequency content show that roller-cone bits produce forces that make them reliable and effective SWD sources to support drilling and exploration activities (see, for instance, Figure 10).

The analysis of PDC-bit dynamics has shown that vertical/axial and lateral vibrations are produced by the drilling action. In particular, large vibrations are produced during transition states and while drilling inhomogeneous formations. A rough estimation of the vibration levels indicates that axial PDC forces are typically more than 10 times lower than the vertical forces of roller bits. Under real drilling conditions, additional vibrations induced by drill-string resonances and mud-pressure modulation also must be evaluated. In general, the P and SV far-field waves radiated in the low seismic frequency are significantly lower in energy than the far-field waves radiated from roller bits. The PDC source may be more similar — for its level in axial and lateral vibrations — to some minivibrators, using loadings of a few kilonewtons (e.g., nominal 2500 lb-force). This source size can be successfully used for investigating distances of several hundred meters. Results obtained in SWD applications indicate that PDC data may be detected by downhole acquisition (Poletto et al., 1997). When the PDC source is assumed as a downhole (instantaneous) polarized single force, the resultant of the lateral and axial components, the energy radiated by the polarized force can be calculated with the same analysis used for

Table 2. Radiation properties of drill-bit and conventional VSP sources.

Source	Drill-bit SWD	Vibroseis	Air gun
Application	Onshore-offshore	Onshore	Offshore (onshore)
Excitation	Vertical force	Vertical force	Pressure pulse
P-waves[1]	8.8%	6.9%	100% (<100%)
S-waves[1]	91.2%	25.8%	0
Surface waves[1]	0	67.3%	0 (>0)
Radiation pattern	Lobed	Lobed	Spherical
Performance specifications	$[(2\pi \text{ rpm} \times \text{TOB})/60] + [(\text{ROP} \times \text{WOB})/3600]$	Peak force	Pressure × volume
Vertical force F_0, F_s (peak to peak)/2	$0 \le 2 \times F_0 \le 3.5$ WOB WOB ~ 100–200 kN	$2 \times F_s \sim 140$–280 kN $F_s \times$ no. vibrators	N/A
P-radiated power	$W_\alpha^{\text{bit}} = \frac{1}{6}\frac{\omega^2 F_0^2}{4\pi\rho\alpha^3}$	$W_\alpha^{\text{vibro}} = \frac{1}{3}\frac{\omega^2 F_s^2}{4\pi\rho\alpha^3}$	See P-radiated energy
Vertical stack	$n_{\text{rec}} \sim \text{hours}/\tau_{\text{rec}}$	$n_{\text{sweep}} \sim \text{minutes}/\tau_{\text{sweep}}$	$n_{\text{shot}} \sim 4$
P-radiated energy	$W_\alpha^{\text{bit}}\tau_{\text{rec}} n_{\text{rec}}$ at given F_0, $\omega = \omega_{\text{bit}}$	$W_\alpha^{\text{vibro}}\tau_{\text{sweep}} n_{\text{sweep}}$ at given F_s, $\omega = \hat{\omega}^2$	From Rayleigh-Willis tables (Dobrin, 1981)
Near-surface energy losses	None	Depend on baseplate coupling and near-surface effects	Losses for bubble effects (tank effects)

[1]Values represent the mean flux of radiated energy and are calculated as a percentage of the total mean flux in the formation assumed as a Poisson's medium.

[2]For a linear sweep, $\hat{\omega}^2 = \omega_{\text{end}}\omega_{\text{start}} + \frac{(\omega_{\text{end}} - \omega_{\text{start}})^2}{3}$.

the vertical single-source model. Moreover, a large spectrum for the action of all single-cutter forces, including rock breaking and possible crack propagation, may be expected at locations close to the bit. Thus, the PDC-bit signal could prove to be a good seismic source for downhole, short-range, high-resolution acoustic investigations. Table 2 summarizes the expected radiation properties of drill-bit and conventional VSP sources as functions of key working parameters.

CONCLUSIONS

The vibration properties and frequency of roller-cone and PDC bits are investigated by considering the main drilling-excitation modes. The analysis shows that the roller-cone drill bit can be used as an energetic wideband source excited by teeth indention and lobed patterns, with periodic and random components modulated in frequency by the drill-string torsional pendulum. The PDC bit is characterized by lower axial and lateral vibration components that produce a lobe-shaped bottom hole. PDC single-cutter impacts are investigated for different drilling conditions and bit geometry. Finally, the radiation of conventional vibrators and other surface sources are numerically calculated and compared with the drill-bit vibration levels to achieve a general understanding of the energy content of SWD data obtained in general drilling and geologic conditions.

ACKNOWLEDGMENTS

The author thanks Klaus Helbig for his valuable suggestions and comments, Anthony Gangi for critical reading and many important comments on the work, and Giorgia Pinna for help in the bibliographic research. The author also thanks ENI-AGIP for supporting the research and for permission to publish the data contained in this article.

APPENDIX A

TORSIONAL MODULATION OF AXIAL VIBRATIONS

Let us consider only the fundamental drill-string torsional mode (also called pendulum mode) of frequency ω_0 and a three-lobe pattern excitation of frequency ω_{ax}, where the subscript ax stands for axial. The angle of the axial-displacement vibration coupled to the torsional mode at the drill bit can be expressed as [equations 23 and 24 in Aarrestad and Kyllingstad (1988)]

$$\varphi_b = \omega_{ax} t \left(1 + A_0 \frac{\sin \omega_0 t}{\omega_0 t}\right). \tag{A-1}$$

The axial displacement can be expressed as

$$u = u_0 \sin\left[\omega_{ax} t \left(1 + A_0 \frac{\sin \omega_0 t}{\omega_0 t}\right)\right], \tag{A-2}$$

where the lobe-pattern frequency is approximated by $\omega_{ax} = 3\omega_{rev} = \pi \text{rpm}_{av}/10$, with rpm_{av} being the average rotary speed. Note that bit rotation–stopping and reverse-spinning effects appear when $A_0 \ge 1$. Aarrestad and Kyllingstad (1988) measure $A_0 \sim 0.3$ in full-scale experiments. The pendulum frequency can be calculated as

$$\omega_0 = 2\pi f_0 = \sqrt{\frac{S}{J}}, \tag{A-3}$$

where S is the static torsional stiffness and J is the effective inertia of the drill string. For a drill pipe of length L_{pipe} and a drill collar of length L_{DC}, the inertia J can be approximated as

(Kyllingstad and Hasley, 1987)

$$J = \rho_1 \left(\frac{I_{\text{pipe}} L_{\text{pipe}}}{3} + I_{\text{DC}} L_{\text{DC}} \right), \qquad \text{(A-4)}$$

where ρ_1 is steel density and where I_{pipe} and I_{DC} are the polar moment of inertia per unit length and mass of drill pipe and collars, respectively. The torsional stiffness S is approximated by

$$S = \frac{\mu I_{\text{pipe}}}{L_{\text{pipe}}}, \qquad \text{(A-5)}$$

where μ is the steel shear modulus. Since the fundamental frequency f_0 is on the order of 0.1 Hz, the frequency modulation index, $A_0\omega_{ax}/\omega_0$ is typically larger than one. The frequency-modulation effect introduces harmonic components at frequencies $\omega_{ax} \pm n\omega_0$ (n integer) as well as large changes in the downhole rpm and torque spectrum (torque is assumed to be proportional to the twist angle between the surface and the bit). During drilling, the string can be twisted several turns, with torque on bit between 0.5 and 10 kNm (Jansen et al., 1995).

REFERENCES

Aarrestad, T. V., and Å. Kyllingstad, 1988, An experimental and theoretical study of a coupling mechanism between longitudinal and torsional drillstring vibrations at the bit: SPE Drilling Engineering, Paper No. 15563.

Adams, N. J., and T. Charrier, 1985, Drilling engineering—A complete well planning approach: PennWell Publishing Company.

Baeten, G., and A. Ziolkowski, 1990, The vibroseis source: Elsevier Science Publ. Co., Inc.

Behr, S. M., T. M. Warren, L. A. Sinor, and J. F. Brett, 1993, 3D PDC bit model predicts higher cutter loads: SPE Drilling & Completion, December, SPE Paper No. 21928.

Biggs, M. D., J. B. Cheatham Jr., and U. Rice, 1969, Theoretical forces for prescribed motion of a roller bit: SPE Paper No. 2391.

Brett, J. F., T. M. Warren, and S. Behr, 1990, Bit whirl—A new theory of PDC bit failure: SPE Drilling Engineering, SPE Paper No. 19571.

Burgess, T. M., and W. G. Lesso Jr., 1985, Measuring the wear of milled tooth bits using MWD torque and weight-on-bit: SPE/IADC Paper No. 13475.

Cassand, J., and M. Lavergne, 1971, Seismic emission by vibrators: *in* Robert Van Nostrand, ed., Seismic filtering: SEG, Translations of Editions Technip, 198.

Chen, S. L., K. Blackwood, and E. Lamine, 1999, Field investigation of the effects of stick-slip, lateral, and whirl vibrations on roller cone bit performance: SPE Paper No. 56439.

Cooley, C. H., P. E. Pastusek, and L. A. Sinor, 1992, The design and desting of anti-whirl bits: SPE Paper No. 24586.

Cunningham, R. A., 1968, Analysis of downhole measurements of drill string forces and motions: Journal of Engineering for Industry, Transactions of the ASME, Series B, **90**, 209–216.

Dareing, D. W., 1982, Drill collar lengths is a major factor in vibration control: SPE Paper No. 11228.

Deily, F. H., D. W. Dareing, G. H. Paff, J. E. Ortloff, and R. D. Lynn, 1968, Downhole measurements of drill string forces and motions: Journal of Engineering for Industry, Transactions of the ASME, Series B, **90**, 217–225.

Devereux, S., 1999, Drilling technology in nontechnical language: PennWell Publishing Company.

Dobrin, M. B., 1981, Introduction to geophysical prospecting, 3rd ed.: McGraw-Hill International Book Company.

Duc, N. Guyen Minh, H. Cholet, and P. Tricot, 1972, Stress concentration induced in elastic rocks under a diamond bit tooth: SPE Paper No. 3987.

Eronini, I. E., W. H. Sommerton, and D. M. Auslander, 1982, A dynamic model for rotary rock drilling: ASME Journal of Energy Resources Technology, **104**, 108–120.

Falconer, I. G., T. M. Burgess, and M. C. Sheppard, 1988, Separating bit and lithology effects from drilling mechanics data: IADC/SPE Paper No. 17191.

Gabolde, G., and J. P. Nguyen, 1999, Drilling data handbook, 7th ed.: Editions Technip.

Glowka, D. A., 1986, The use of single-cutter data in the analysis of PDC bit design: SPE Paper No. 15619.

Hanson, J. M., and W. R. Hansen, 1995, Dynamics modeling of PDC bits: SPE/IADC Paper No. 29401.

Hardage, B. A., 1992, Crosswell seismology and reverse VSP: Geophysical Press.

Hasley, G. W., Å. Kyllingstad, T. V. Aarrestad, and D. Lysne, 1986, Drillstring torsional vibrations: Comparison between theory and experiment on full-scale research drilling rig: SPE Paper No. 15564.

Holster, J. L., and R. J. Kipp, 1984, Effect of bit hydraulic horsepower on the drilling rate of a polycrystalline diamond compact bit: Journal of Petroleum Technology, SPE Paper No. 11949, 2110–2118.

Hutchinson, M., V. Dubinsky, and H. Henneuse, 1995, An MWD downhole assistant driller: SPE Paper No. 30523.

Jansen, J. D., L. van den Steen, and L. Zachariasen, 1995, Active damping of torsional drillstring vibrations with a hydraulic top drive: SPE Drilling & Completion, SPE Paper No. 28911, 250–254.

Jardine, S. I., M. L. Lesage, and D. P. McCann, 1990, Estimating tooth wear from roller cone bit vibration: IADC/SPE Paper No. 19966.

Kyllingstad, Å., and G. W. Hasley, 1987, A study of slip-stick motion of the bit: SPE Paper No. 16659.

Langenkamp, R. D., 1994, Illustrated petroleum reference dictionary, 4th ed.: PennWell Publishing Company.

Langeveld, C. J., 1992a, PDC bit dynamics: IADC/SPE Paper No. 23867.

———, 1992b, PDC bit dynamics (Supplement to IADC/SPE Paper No. 23867): IADC/SPE Paper No. 23873.

Ma, D., and J. J. Azar, 1985, Dynamics of roller cone bits: Journal of Energy Resources Technology, Transactions of the American Institute of Mechanical Engineers, **107**, 543–548.

Ma, D., D. Zhou, and R. Deng, 1995, The computer simulation of the interaction between roller bit and rock: SPE Paper No. 29922.

McGehee, D. Y., J. S. Dahlem, J. C. Gieck, B. Kost, D. Lafuze, C. H. Reinsvold, and S. C. Steinke, 1992a, The IADC roller bit classification system: IADC/SPE Paper No. 23937.

———, 1992b, The IADC roller bit dull grading system: IADC/SPE Paper No. 23938.

Miller, G. F., and H. Pursey, 1954, The field and radiation impedance of mechanical radiators on the free surface of semi-infinite isotropic solid: Proceedings of the Royal Society, **223**, 521–541.

Miranda, F., L. Aleotti, F. Abramo, F. Poletto, A. Craglietto, S. Persoglia, and F. Rocca, 1996, Impact of seismic while drilling technique on exploration wells: First Break, **14**, 55–68.

Naganawa, S., S. Tanaka, and N. Sugaya, 1995, Experimental and theoretical analysis of roller cone bit vibrations: Energy Sources Technology Conference, American Society of Mechanical Engineers, Proceedings, 1–7.

Poletto, F., 2005, Energy balance of a drill-bit seismic source, part I: Rotary energy and radiation properties: Geophysics, this issue.

Poletto, F., M. Malusa, and F. Miranda, 2001, Numerical modeling and interpretation of drill-string waves: Geophysics, **66**, 1569–1581.

Poletto, F., F. Miranda, P. Corubolo, and F. Abramo, 1997, Seismic while drilling using PDC signals — Seisbit experience and perspectives: 59th Annual International Meeting, EAGE, Extended Abstracts, E-053.

Rector III, J. W., and B. P. Marion, 1991, The use of drill-bit energy as a downhole seismic source: Geophysics, **56**, 628–634.

Santos, H., J. C. R. Plácido, and C. Wolter, 1999, Consequences and relevances of drillstring vibration on wellbore stability: SPE/IADC Paper No. 52820.

Sheppard, M. C., and M. Lesage, 1988, The forces at the teeth of a drilling rollercone bit: Theory and experiment: SPE Paper No. 18042.

Skaugen, E., 1987, The effects of quasi-random drill bit vibrations upon drillstring dynamic behavior: SPE Paper No. 16660.

White, D. B., and D. A. Curry, 1988, Effects of nozzle configuration on roller cone bit performance: IADC/SPE Paper No. 17188.

Winters, W. J., T. M. Warren, and E. C. Onyia, 1987, Roller bit model with rock ductility and cone offset: SPE Paper No. 16696.

Wolf, S. F., M. Zacksenhouse, and A. Arian, 1985, Field measurements of downhole drillstring vibrations: SPE Paper No. 14330.

Yang, L. Z., 1990, The analysis of relations between a tricone bit and lobed bottom in low frequency axial vibration: SPE Paper No. 20325.

Zijsling, D. H., 1987, Single cutter testing — A key for PDC bit development: SPE Paper No. 16529/1.